Anisotropic strength in discontinuity layout optimisation for undrained slope stability analysis

Citation for the original published paper (version of record):
Sellin, C., Abed, A., Karlsson, M. et al (2025). Anisotropic strength in discontinuity layout optimisation for undrained slope stability analysis. Canadian Geotechnical Journal, 62.
http://dx.doi.org/10.1139/cgj-2024-0541

(article starts on next page)

Canadian Geotechnical Journal

OPEN ACCESS | Research Article

Anisotropic strength in discontinuity layout optimisation for undrained slope stability analysis

Carolina Sellin[a,b], **Ayman Abed**[a], **Mats Karlsson**[a], **Jelke Dijkstra**[a], and **Colin Campbell Smith**[c]

[a]Department of Architecture and Civil Engineering, Chalmers University of Technology, Sven Hultins gata 6, Gothenburg SE-412 96, Sweden; [b]Swedish Geotechnical Institute, Hugo Grauers gata 5B, Gothenburg SE-412 96, Sweden; [c]School of Mechanical, Aerospace & Civil Engineering, University of Sheffield, Mappin Street, Sheffield S1 3JD, United Kingdom

Corresponding author: **Ayman Abed** (email: ayman.abed@chalmers.se)

Abstract

Slope stability analysis in 2D ranges from the classical and conventional limit equilibrium method to the robust and computationally demanding finite element (FE) analysis. Discontinuity layout optimisation (DLO) is an interesting intermediate method that applies an upper bound limit analysis with the assumption of rigid-perfectly plastic soil behaviour. Here, the whole soil mass is discretized using a set of potential slip-lines and optimisation is used to identify the critical mechanism that can be formed from a subset of these lines that dissipates the least energy. This method has only been used for isotropic soil models, except for rare studies that included an anisotropic model. This paper introduces the use of an anisotropic failure criterion in DLO, based on the total stress-based NGI-ADP model. The performance of DLO with this simplified NGI-ADP model is compared with respect to failure mechanism and safety factor determined by corresponding FE analysis. The results show good agreement between the two methods and highlight the use of DLO as a powerful method with straightforward input parameters and low computational time for slope stability assessment.

Key words: slope stability, anisotropy, limit analysis, upper bound, safety factor

Résumé

L'analyse de la stabilité des pentes en 2D va de la méthode classique et conventionnelle de l'équilibre limite (LEM) à l'analyse par éléments finis (EF), à la fois robuste et exigeante sur le plan informatique. L'optimisation de l'implantation par discontinuités (DLO) est une méthode intermédiaire intéressante qui applique une analyse limite supérieure en supposant un comportement de sol rigide parfaitement plastique. Ici, l'ensemble de la masse de sol est discrétisé à l'aide d'un ensemble de lignes de glissement potentielles, et une optimisation est utilisée pour identifier le mécanisme critique pouvant être formé à partir d'un sous-ensemble de ces lignes qui dissipent le moins d'énergie. Cette méthode n'a été utilisée que pour des modèles de sol isotropes, à l'exception de rares études ayant inclus un modèle anisotrope. Cet article présente l'utilisation d'un critère de défaillance anisotrope dans la méthode DLO, fondé sur le modèle NGI-ADP basé sur les contraintes totales. La performance de la méthode DLO avec ce modèle NGI-ADP simplifié est comparée en termes de mécanisme de rupture et de facteur de sécurité déterminé par l'analyse EF correspondante. Les résultats montrent une bonne concordance entre les deux méthodes et mettent en évidence l'utilisation de la méthode DLO comme une approche puissante, avec des paramètres d'entrée simples et un temps de calcul réduit pour l'évaluation de la stabilité des pentes.

Mots-clés : stabilité des pentes, anisotropie, analyse limite, limite supérieure, facteur de sécurité

1. Introduction

The use of appropriate models for slope stability assessment is crucial for understanding and avoiding slope failures, with shear strength being the most influential soil property in these analyses. The level of simplification of the physical mechanisms acting on a slope dictates the complexity of the modelling approach; for example, limit analysis is a powerful tool to assess stability. Rigorously speaking, in its most basic form, this ultimate limit state (ULS) problem requires developing lower and upper bound approximations while assuming rigid-perfectly plastic soil behaviour. However, a conventional method for stability analyses commonly used in engineering practice is the limit equilibrium method (LEM) (Fellenius 1926; Bishop 1955; Morgenstern and Price 1965; Spencer 1967), which is, in general, neither an upper nor a lower bound solution (Yu et al. 1998). The attraction lies in the simplified mechanisms that need to be evaluated, but with the drawback of the need of a priori assumptions for the failure mechanism and the inter-slice forces. These simplifications can become problematic when anisotropic behaviour of the soil strength and complex slope geometries need to be accounted for. One of the most comprehensive alternatives that overcomes the limitations of LEM is therefore finite element (FE) analysis with strength reduction method (SRM) (Zienkiewicz et al. 1975; Griffiths and Lane 1999), which instead discretises the complete soil mass. The FE-based method satisfies both the force equilibrium equations and the kinematics and allows for advanced (total- and effective stress-based) constitutive models to be employed. This refinement comes at the expense of more demands to the user, in terms of time and knowledge for setting up the model, interpretation of results, and increased computational time. However, on one hand, with the current computing capabilities, FE analysis is not ideal for stability assessments on a regional scale, where 2D evaluations must be automated for high computational efficiency (in terms of the number of analyses per time unit). On the other hand, LEM is limited by the uncertainties associated with the assumed failure surface and the assumptions regarding interslice forces. In this context, the discontinuity layout optimisation (DLO) (Smith and Gilbert 2007) offers a strong alternative, balancing the strengths of both LEM and finite element method (FEM) in terms of generality, complexity, and computation time.

DLO is an upper bound limit analysis (LA) method that, in contrast to LEM, satisfies global force equilibrium (Michalowski 1989) and seeks a solution where the energy dissipation rate exceeds the rate of work. DLO specifically identifies the critical failure mechanism using optimisation, but simplifies the soil behaviour within the LA-framework to perfectly plastic. Hence, DLO also allows for a slip-line-based discretisation, rather than the more computationally demanding and mesh-dependent FE-based option (Sloan 2013). Until now, the DLO framework only incorporated isotropic soil strength.

The readily available implementation of DLO in LimitState:GEO has been verified against analytical solutions, upper and lower bound LA and FE analyses by, for example, Smith and Gilbert (2007), and Zheng et al. (2019) and used for verification of analytical or LE-based methods (Vahedifard et al. 2016; Yang et al. 2019; Zheng et al. 2020), but comparisons of DLO with FE stability analyses are rare. The few cases that exist include Gourvenec and Mana (2011), Zhou et al. (2018*a*), and Zheng et al. (2019), who studied the performance of DLO in bearing capacity problems against total stress FE-analyses and effective stress FE-analyses reported in literature (Loukidis et al. 2008; Lee et al. 2014), respectively. Similarly, Leshchinsky (2015) and Zhou et al. (2018*b*) both compared bearing capacities and failure mechanisms of footings on slope crests calculated with DLO against FE-analyses from literature (Georgiadis 2010). The five studies showed generally very good agreement in the bearing capacity factor between the methods. The effectiveness of DLO in simulating the stability of reinforced soil has also been demonstrated in both embankments (Smith and Tatari 2016) and slopes (Liang and Knappett 2017) through comparisons with analytical solutions as well as LE and FE analyses reported in the literature (Hird 1986; Rowe and Soderman 1987; Jewell 1988; Rowe and Li 1999). Also here, the results showed good agreement, where the former study additionally showed that DLO could detect more critical failure mechanisms. The latter study, on the other hand, expanded DLO to include the effect of vegetation and found good agreement with centrifuge tests. For conventional slope stability analysis though, the comparisons are based on LE (Leshchinsky 2013; Leshchinsky and Ambauen 2015) alone, with generally good agreement in safety factor and failure mechanism and with DLO for some cases identifying a more critical failure mechanism. Notably, Crumpton (2020) presented an initial effort to integrate an anisotropic material model into DLO for analysing slope stability.

This paper presents a comprehensive verification of an implementation of the anisotropic total stress-based NGI-ADP model (Grimstad et al. 2012) into a research version of LimitState:GEO 3.7, for slope stability analyses. Practically, DLO represents an advancement from the commonly used LE method, by combining the strength of discretising the whole soil mass, as in FE analysis, and thereby avoiding a priori assumptions and the ability to implement advanced strength models while preserving the simple input, the fast calculations, numerical stability, and the ease of use, typical for LE. The verification is carried out against reference results of the commercially available implementation of NGI-ADP in the commercial Finite Element code PLAXIS 2D.

2. Limit analysis and DLO

Limit analysis (LA) idealises the soil behaviour to rigid-perfectly plastic and applies an associated flow rule. Thereby, similar to LE, LA only allows for assessing ULS with the inherent simplification of a constant mobilisation of the strength along the shear band, but LA is more robust since it requires fewer assumptions about static equilibrium (Leshchinsky and Ambauen 2015). LA consists of a lower and upper bound plasticity theorem, where the former must satisfy equilibrium and boundary conditions while not violating the failure criterion at any point within the soil mass. Intuitively, the theorem of the upper bound satisfies the global force equilibrium equations (Michalowski 1989) and seeks to obtain an upper bound for a kinematically acceptable failure surface, given the rate of work (energy dissipation). The upper bound solution can thereby be seen as a special, rigorous, case of LE, but notably not vice versa (Mróz and Drescher 1969; Yu et al. 1998).

Yield is only checked in part of the domain in an upper bound solution, as discussed by Smith and Gilbert (2022), and the mechanism of failure is not necessarily the most critical failure mechanism. An optimisation process is therefore required to identify the most critical failure mechanism (Smith and Gilbert 2007).

There is a clear advantage in discretising the soil mass when performing LA to avoid a priori assumptions of the failure mode. The corresponding discretisation using continuum mechanics (FE) suffers from the inherent problem of mesh-dependent width of the shear band, which requires additional mesh-adaptation (Sloan 2013). To mitigate this, modern FE LA implementations often incorporate velocity discontinuities between adjacent elements, allowing localized shear bands to be captured without excessive mesh refine-

Can. Geotech. J. **62:** 1–16 (2025) | dx.doi.org/10.1139/cgj-2024-0541

Fig. 1. Stages of (*a–c*) discretisation and (*d*) calculation of soil mass in discontinuity layout optimisation. Based on Gilbert et al. (2010).

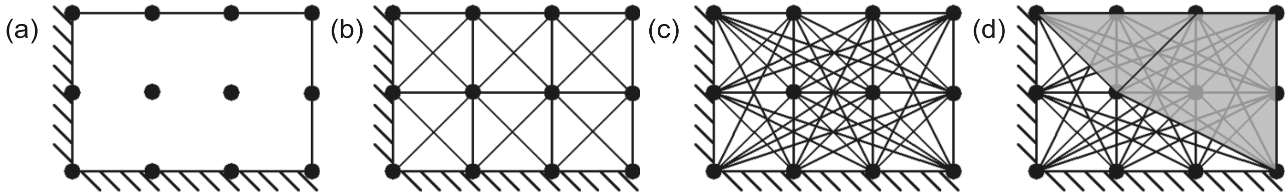

ment (Krabbenhøft 2023). This is avoided in DLO by discretising the soil mass into nodes connected by slip-lines, resulting in an infinitely thin shear band. The drawback of using linear slip-lines is the default restriction to translational slips of the individual blocks, which in general can closely simulate global rotational failure of the type seen in slope stability problems. Smith and Gilbert (2013) have successfully added the possibility for linear and curved slip-lines, which allow for greater precision, especially for problems with significant imposed external moment loading. In contrast this work only considers the commercially available translational version.

The numerical analysis procedure in DLO (Smith and Gilbert 2007) is summarised in Fig. 1; (a) user-defined distribution of nodes; (b and c) node-to-node slip-lines generated, either restricted to (b) adjacent nodes or to (c) all nodes, depending on the solution strategy adopted; (d) optimisation to identify the combination of slip-lines that generates a collapse mechanism that dissipates the least energy. This is returned together with the factor on load (soil self-weight) needed to generate this collapse mechanism.

One of the key features of DLO is the long slip-lines, which are allowed to intersect, with the result of a large amount of potential sliding blocks. Given n nodes, the total number of slip-lines is approximately $m = n \cdot (n - 1)/2$ (Smith and Gilbert 2007). This can, however, become computationally demanding for larger geometries and/or high nodal densities, which has been solved by an intermediate computational step; Fig. 1*b*. Here, the upper bound solution is computed only for short slip-lines. The obtained (low accuracy) solution is used as input for searching all potential slip-lines, m (Fig. 1*c*), to find the ones that violate the failure criterion. Only the slip-lines that violate the failure criterion will be added to the problem, followed by a new computation of the upper bound solution. This iterative, adaptive method is continued until the failure criterion no longer results in more slip-lines, followed by applied strength reduction to obtain the final solution in Fig. 1*d*.

The critical failure mode for undrained conditions, and corresponding safety factor, is obtained using the SRM with eq. 1:

$$F = \frac{s_u}{s_{u,r}} \tag{1}$$

where s_u is the available undrained soil strength and $s_{u,r}$ is the mobilised undrained soil strength at failure. The value of $s_{u,r}$ is determined by an iterative reduction of s_u until non-convergence is reached (FE) (Zienkiewicz et al. 1975) or a combination of slip-lines that violate the (updated) failure criterion (DLO) is obtained. Alternatively for DLO problems with undrained materials and no external loads, the factor on strength is identical to the factor on soil self-weight, and the strength reduction phase can be omitted.

3. NGI-ADP model

The total stress-based NGI-ADP model by Grimstad et al. (2012) is an anisotropic modification of the Tresca yield criterion, as first proposed by Davis and Christian (1971). The anisotropic behaviour is included as a shift of the Tresca centre line in the deviatoric plane, using the concept of ADP (Bjerrum 1973) with an active (A, stress rotation $\beta = 0$), direct (D, β assumed to be 30°), and passive (P, $\beta = 90°$) zone in plane strain, respectively.

As shown in Fig. 2, the ADP-zones are directly linked to direct simple shear test, triaxial compression (C), and extension (E) test. Experimental results comparing plane strain and triaxial results, as compiled by Ladd et al. (1977), show $s_u^C/s_u^A = 0.87 - 0.97$ and $s_u^E/s_u^P = 0.8 - 0.84$, with the differences originating from the size of the intermediate stress, σ_2. Based on s_u^C/s_u^A, Grimstad et al. (2012) introduces a rounding ratio, 0.97 $\lesssim a_1 < 1.0$, together with a Tresca approximation proposed by Billington (1988) and a modified Von Mises plastic potential function, to avoid inherent numerical issues from sharp corners in the Tresca formulation.

The model is implemented for general stress space in FE, using the modified second and third deviatoric invariants, $\widehat{J_2}$ and $\widehat{J_3}$, see definition in Appendix A. The failure criterion is defined as eq. 2:

$$F = \sqrt{H(\omega)\widehat{J_2}} - \kappa \frac{s_u^A + s_u^P}{2} = 0 \tag{2}$$

where $H(\omega)$ controls the Tresca approximation by eqs. 3 and 4; κ is the strain-dependent hardening parameter in eq. 5. The latter is controlled by the plastic strain, γ^p, and the plastic strain at failure, γ_f^p (Grimstad et al. 2012).

$$H(\omega) = \cos^2\left(\frac{1}{6}\arccos(1 - 2a_1\omega)\right) \tag{3}$$

$$\omega = \frac{27}{4}\frac{\widehat{J_3}^2}{\widehat{J_2}^3} \tag{4}$$

$$\kappa = 2\frac{\sqrt{\gamma^p/\gamma_f^p}}{1 + \gamma^p/\gamma_f^p} \quad \text{for } \gamma^p < \gamma_f^p \quad \text{else } \kappa = 1 \tag{5}$$

Fig. 2. Principal stress directions along a slip surface, based on Lo (1965), Bjerrum (1973), Sambhandharaksa (1977), Ladd et al. (1977), and Zhu et al. (2016).

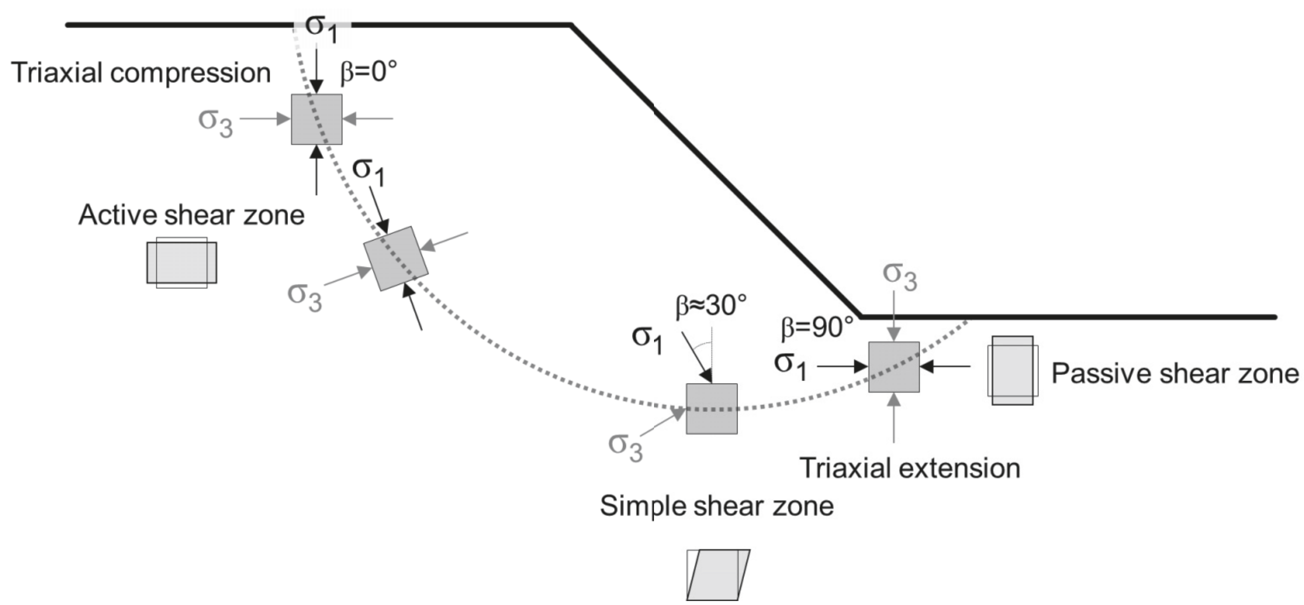

Fig. 3. Failure surfaces in the deviatoric plane, based on Grimstad et al. (2012).

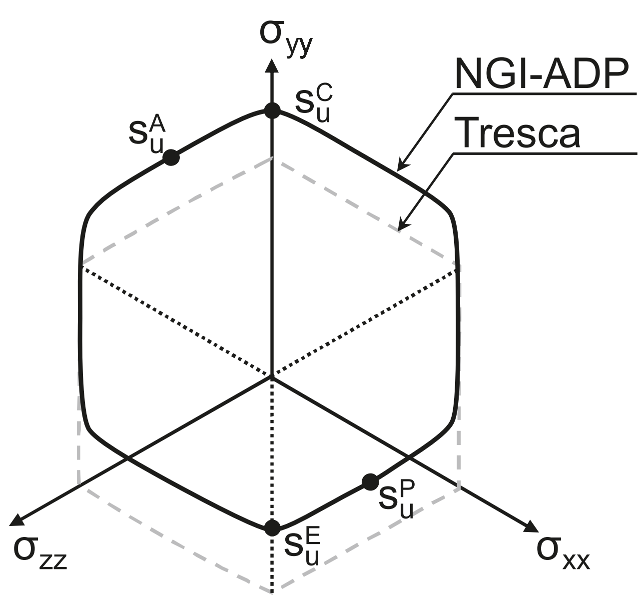

The failure criterion collapses into the Tresca formulation when a_1 approaches 1.0, and is fixed to 0.99 in PLAXIS. In LimitState:GEO, on the other hand, the slip-line discretisation circumvents the problem with numerical singularities allowing for the exact formulation. Figure 3 illustrates the anisotropic modification and the rounding effect in the deviatoric plane. Since strengths obtained from triaxial tests are generally lower than the corresponding value from plane strain tests, the results from triaxial tests can be used directly for the plane strain strength s_u^A and s_u^P, as suggested by Grimstad et al. (2012) and applied in Jostad et al. (2014), Ukritchon and Boonyatee (2015), D'Ignazio et al. (2017), and Li et al. (2022).

The simplified version of NGI-ADP in LimitState:GEO consists of a multiplier, f, that applies to a defined baseline undrained shear strength, here called $s_{u,\text{ base}}$. Just as in FE, LimitState:GEO allows for a linear variation of $s_{u,\text{ base}}$ within the depth of a soil layer. f varies with the inclination of the slip-line, θ, and has a sign dependency to distinguish positive and negative shear:

(6) $$f^+ = F_A \cos(2\theta - 90) + \sqrt{(F_B \cos(2\theta - 90))^2 + (F_D \cos(2\theta))^2}$$

(7) $$f^- = F_A \cos(2\theta + 90) + \sqrt{(F_B \cos(2\theta + 90))^2 + (F_D \cos(2\theta))^2}$$

where

(8) $$F_A = \frac{f_u^A - f_u^P}{2}$$

(9) $$F_B = \frac{f_u^A + f_u^P}{2}$$

(10) $$F_D = f_u^{\text{DSS}}$$

f_u^A, f_u^P, and f_u^{DSS} are given by the user and defined as the multipliers for plane strain undrained shear strength in active, passive, and direct simple shear direction, respectively, e.g. $s_u^A = f_u^A s_{u,\text{base}}$.

The full formulation of NGI-ADP model (in FE) also accounts for stiffness anisotropy, with nonlinear hardening behaviour as a function of the shear strain at failure given different loading directions. This feature is, however, not as relevant for stability assessment of slopes, given the ULS-type of problem, and cannot be included in LA given the assumption of perfectly-plastic soil behaviour.

Fig. 4. Dimensions and boundary conditions with an optional weak layer highlighted.

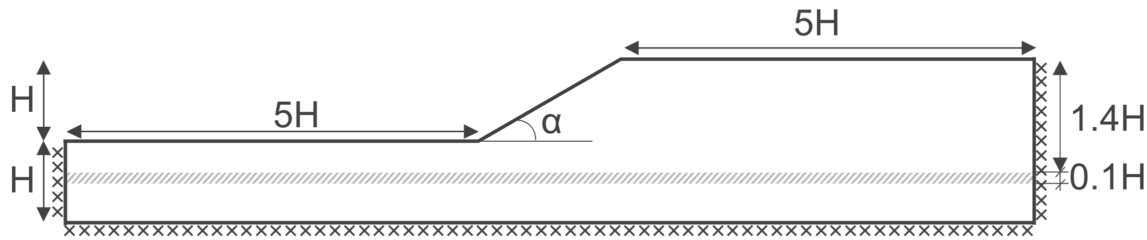

Table 1. Applied shear strengths.

Definition (n)	Abbreviation	Values of n
Isotropic	I	1
s_u^A/s_u^{DSS}	An	1.1, 1.2, 1.3, 1.4, 1.5
s_u^P/s_u^{DSS}	Pn	0.5, 0.6, 0.7, 0.8, 0.9
s_u^A/s_u^{DSS} and $2 - s_u^P/s_u^{DSS}$	APn	1.1, 1.2, 1.3, 1.4, 1.5

4. Stability analyses

4.1. Geometry and parameter variations

A benchmark slope was created to verify the functionality of the NGI-ADP failure criterion in LimitState:GEO against corresponding implementation in PLAXIS 2D and against the same magnitude of anisotropy in the more commonly used LE method with GeoStudio SLOPE/W 2021. The slope dimensions are presented in Fig. 4, with $H = 10$ m and $\alpha = [15°, 90°]$ with 15° increments.

A saturated unit weight of 15 kN/m^3 was constant for all simulations with a default shear strength of s_u^{DSS}= 40 kPa, to avoid resulting safety factors <1.0. The anisotropic shear strength was applied as (1) an increase of s_u^A; (2) a decrease of s_u^P, and (3) a combination of both, in addition to an isotropic reference case, see Table 1. The combination of s_u^A and s_u^P corresponds to $s_u^P/s_u^A = 0.3 - 0.8$, which is in line with the ratios observed by, for example, Karlsrud et al. (2005) using triaxial tests on Norwegian clay and Sambhandharaksa (1977) using plane strain tests on Connecticut varved clay. All 16 shear strength combinations were applied to the six different slope angles, with safety factors from all methods presented in Appendix B.

A sensitivity analysis of the nodal discretisation was conducted for the case of a 30°-slope with a constant s_u^{DSS}, $s_u^A = 1.3s_u^{DSS}$, and $s_u^P = 0.7s_u^{DSS}$, abbreviated according to Table 1 to AP1.3. The safety factor varied <1% between the extremes 250 and 4000 nodes, but an increase in the nodal density resulted in a more circular failure mechanism in the direct- and passive zone (see Fig. Fig. 5). The nodal discretisation was therefore set to a target of 2000 nodes for all geometries, similarly to Leshchinsky and Ambauen (2015).

All shear strength combinations were first applied to slope angle α and $-\alpha$ in LimitState:GEO, resulting in identical safety factors. This confirms that the implementation of the anisotropic strength is independent of the slope direction, in contrast to, for example, the LE software GeoStudio SLOPE/W.

Based upon a separate mesh-convergence study for the finite element calculations, the slope model was discretised into approximately 600 15-noded elements where fewer elements were used for the steepest slope, see Fig. 6 for an example mesh.

4.2. Comparison with LEM

The soil was assumed to have homogeneous strength profile with the anisotropic combinations presented in Table 1. The anisotropy in the LE framework is here included via a user-defined shear strength scale factor to emulate the yield criterion in the NGI-ADP model (see Fig. Fig. 7). Here, the illustrated idealised sinusoidal function was either used for active (A), passive (P), or the combination of them (AP) in analogy with the applied shear strengths in Table 1. The shape of the scale factor originates from the observations on Swedish and Norwegian clay by, for example, Bjerrum (1973) and is commonly used for practical purposes in Sweden (Skredkommissionen 1995).

The critical slip surface from LEM was calculated by assigning a search range for the start- and endpoint of the failure mechanism (so- called entry–exit (EE)–method) with each slip surface discretised with 30 slices. Deviations of the safety factor from LEM, as estimated from the DLO method, are represented as a relative change of the safety factor:

$$\Delta F_{\text{LEM}} = \frac{F_{\text{DLO}} - F_{\text{LEM}}}{F_{\text{LEM}}} \tag{11}$$

The result, presented in Fig. 8 with values of the safety factor shown in Appendix B, shows that the reduction of s_u^P is the main source for deviations from the isotropic case. Results from DLO show a higher safety factor than LEM for α = 15°–30°, and the contrary for steeper slope angles. The discrepancy is not necessarily intuitive, since LEM gives neither a lower nor upper bound solution (Yu et al. 1998). Rather, the observed trend might be explained when examining the critical slip surface in Fig. 9 for AP1.5. Here, the critical failure modes from both methods are in good agreement for shallow slope angles, and the safety factor from DLO can indeed be considered as an upper bound solution. The failure mode for steeper slopes do however differ and the corresponding safety factors show no clear trend in Fig. 8. The effect of the failure mode was further investigated by assigning the exact same slip surface from DLO in LEM for AP1.5. Figure 10 shows the previous linear deviations when using EE method, in comparison to the fully specified (FS) slip surface. With this guidance of failure mode, the safety factors from DLO were

Fig. 5. Slip surfaces using nodal target 250 and 2000. Background nodes have nodal target 2000, and its corresponding failure mode is highlighted together with its individual blocks.

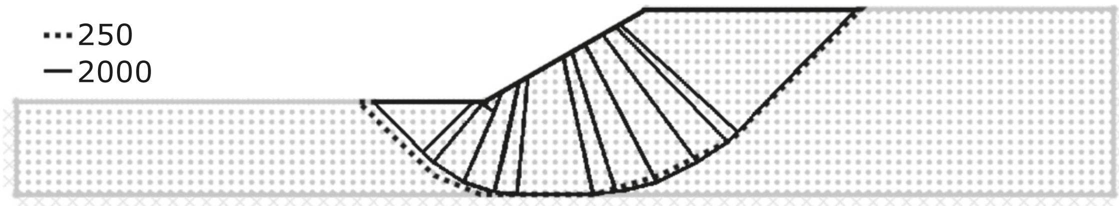

Fig. 6. Example of element distribution used for 30°-slope with finite element.

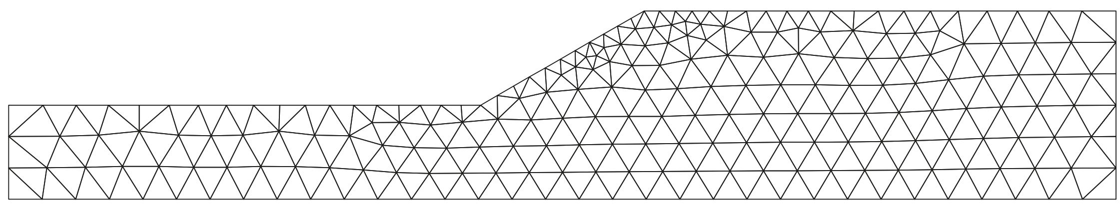

Fig. 7. Anisotropic function used for limit equilibrium method, where θ is the inclination of the failure surface.

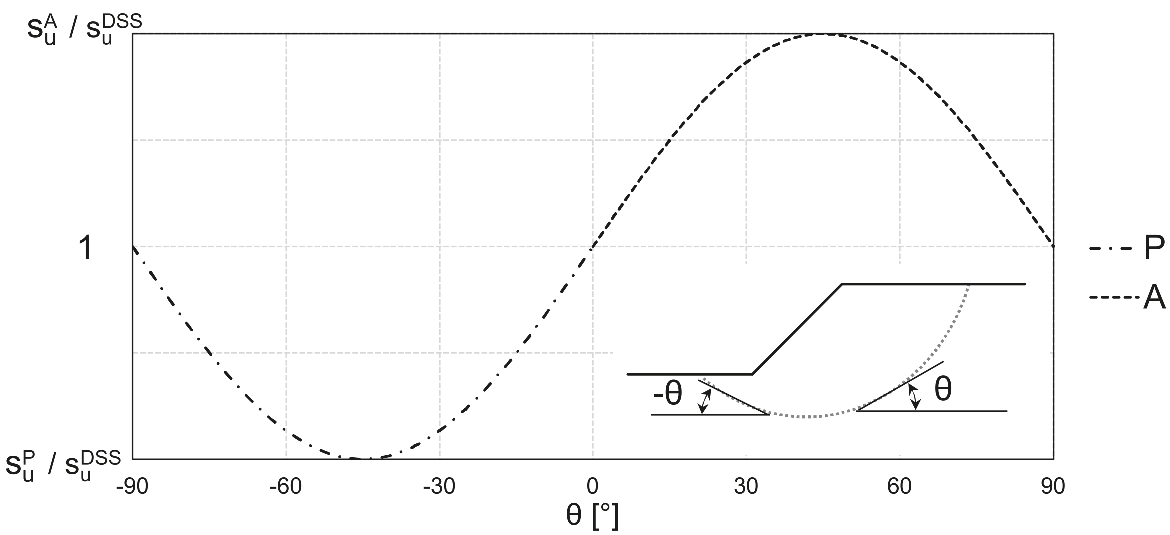

now consistently higher than LEM, even following the trend of the isotropic reference case.

4.3. Comparison with FE

In the following subsections, results from finite element analyses are used as a reference in terms of safety factor and failure mode. Consequently, deviations of the safety factor from the reference are based on eq. 11 with F_{FE} substituting for F_{LEM}.

4.3.1. Constant shear strength with depth

Figure 11 shows the differences between the calculation methods for isotropic and anisotropic (uniform) strength profiles, with values of the safety factor shown in Appendix B. Both Figs. 11*a* and 11*b* have a constant s_u^{DSS} with depth, with various anisotropic factors. All anisotropic combinations show that the safety factors from DLO have good agreement with the corresponding F_{FE} results, with deviations of up to 5% and the largest deviations occurring for gentle slopes. The same behaviour and magnitude is seen for the isotropic case, as shown in Fig. 11. As can be expected for the upper bound nature, the DLO results, with some exceptions, systematically fall above those obtained for FE. In all cases, the small deviations are noticeably increasing with increasing anisotropy in the active shear zone (s_u^A) for 30°–45° slopes. This behaviour is corroborated by the shape of the failure modes in Fig. 12, where the effect is most prominent close to the slope crest. Results from FE show a thick circular shear zone, whereas DLO instead has a single slip-line, independent of the nodal density, as illustrated in Fig. 5.

4.3.2. Linear increase of shear strength

Incorporating a linear increase of s_u^{DSS} with 1 kPa/m below the slope crest, simulating normally consolidated clays, re-

Fig. 8. Difference in safety factors between discontinuity layout optimisation and limit equilibrium method for anisotropy applied on (*a*) s_u^A or s_u^P; (*b*) s_u^A and s_u^P.

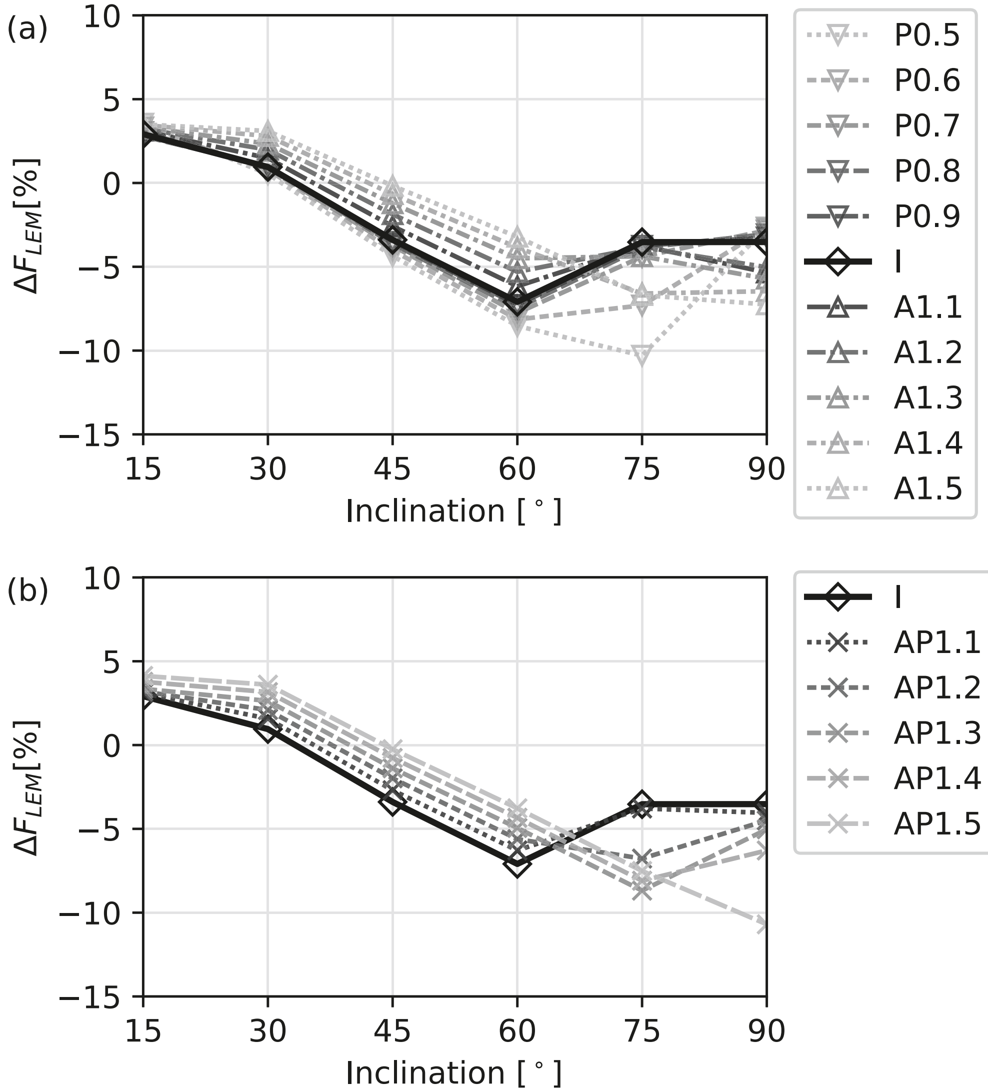

Fig. 9. Failure modes from discontinuity layout optimisation (solid lines) and limit equilibrium method (grey shade) for AP1.5.

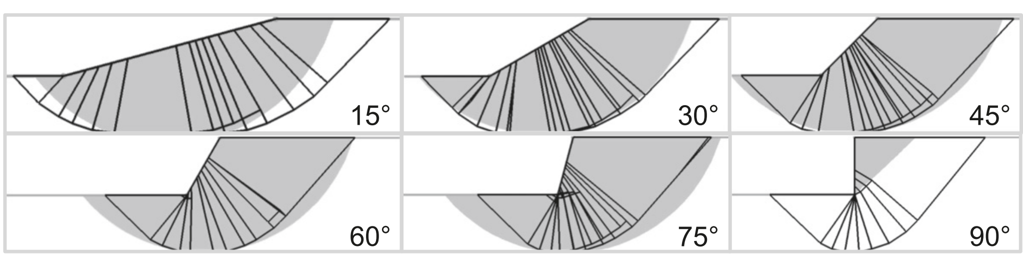

sulted in the differences shown in Fig. 13 with safety factors shown in Appendix B. The same behaviour and magnitudes in variation is seen here as in Fig. 11, but with values in closer agreement to the isotropic case.

The close agreement can be traced to the combination of the level-dependent undrained strength, a well-known simplification of the (vertical) effective-stress based shear strength, and the given anisotropy obtained from principal stress-rotation along the failure. Mathematically, the depth-dependent undrained strength reduces the effect of anisotropy, see Fig. D1 in Appendix D.

4.3.3. Linear increase of shear strength with a weak layer

The influence of a weak layer was investigated, see geometry in Fig. 4, with an increased mesh density in the FE model, as shown in Fig. 14. In DLO, the weak layer had the same

Fig. 10. Difference in safety factors between discontinuity layout optimisation and limit equilibrium method.

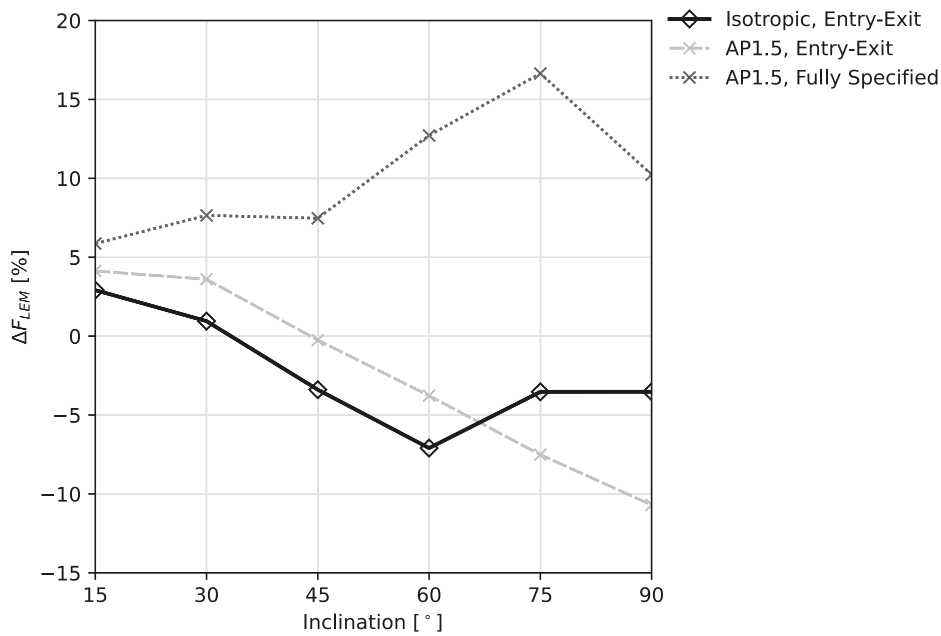

nodal density as the other scenarios, with the default 0.5 m nodal spacing along the boundaries. Three additional internal boundaries were added to allow for internal rotational failures, as further explained in Appendix C.

The weak layer was chosen to have the same density as the soil mass, and a 10-fold reduced undrained shear strength, $0.1s_u^{\mathrm{DSS}}$, without anisotropy.

The location and orientation of the weak layer did not affect the deviation from the isotropic reference case, as seen in Fig. 15. Evidently, both FE and DLO calculate a wider, partially circular, failure mode in the active shear zone for 30°–60° slopes, shown in Fig. 16, and as the slope angle increase further, the failure modes coalesce. The wide failure mode from DLO stems from the inclusion of the (rotational) internal boundaries, which also result in minimal deviations in the safety factor from the corresponding FE analysis. The location of the inclined internal boundary is clearly the most influential, with its effect on the obtained safety factor being reduced in the 60° slope where the boundary is located outside the FE failure mode. This effect is more prominent in the 75° slope, where the DLO cannot capture the wide failure mode and the resulting deviation in safety factor is increasing. It should be noted that some combinations of anisotropy and slope inclination did not converge to a solution in LimitState:GEO using strength reduction. There, instead, the results were obtained using increased soil weight. A few combinations also resulted in different values from strength reduction and increased soil weight, where the latter one was chosen, the preconditions of all safety factors are presented in Appendix B.

4.4. General observations on the upper bound solution from DLO

The simulations show that, as anticipated, DLO results in a safety factor equal to or higher than the reference with FEM for $15^\circ \leq \alpha \leq 75^\circ$, when the failure mode is nonrestricted. For slope angles >75°, however, DLO results in a slightly lower safety factor than FEM, although with less than a 5 percentage point deviation. The difference between the methods was the least when the failure mode was constrained by a weak layer. This special case included an increased mesh density in the weak layer in FEM and added boundaries in DLO to allow for rotational failures, clearly improving the results. The slight difference still occurring between the methods stems from the restriction of linear slip lines in DLO. As the undrained shear strength is reduced during safety analysis, the energy dissipation rate and displacement rate increase, and the individual blocks (given slip-lines) move *independently*. That is in contrast to FEM, where the elements are coupled and results in a continuous failure mode. This difference between methods is of no concern for (nearly) closed form solutions with slope angle $\alpha = 15^\circ$ and 90°, where the failure shape from FE analysis is parallel to the obtained (translational) slip-line. However, for $\alpha > 15^\circ$, FE analyses capture a more circular shape, which gradually turns translational for increasing slope angles. It is anticipated that this is related to the use of (primarily) translational only DLO model and that extending the analysis to include rotational deformations would bring greater convergence to the results. However, for most studied problems, this seems to add unnecessary complexity. On the contrary, a safety factor is the result of a chain of uncertainties. The uncertainty of the undrained shear strength alone is minimum 10% (Phoon and Kulhawy 1999), while the maximum difference between F_{DLO} and F_{FEM} for the investigated cases was maximum 5%. Thus, in most practical cases, the DLO results can be relied upon directly. However, if the safety factor values are within 5% of the borderline for specific practical requirements, it is advisable to perform an additional check using FEM.

Finally, the simulations were performed on a standard laptop PC with 1.80/4.8 GHz Intel Core i7-1265U and 32 GB memory. For the case with constant shear strength with depth, the

 Can. Geotech. J. 62: 1–16 (2025) | dx.doi.org/10.1139/cgj-2024-0541

Fig. 11. Difference in safety factor between discontinuity layout optimisation and limit equilibrium method for homogeneous soil with varying slope inclination for anisotropy applied on (*a*) s_u^A or s_u^P; (*b*) s_u^A and s_u^P.

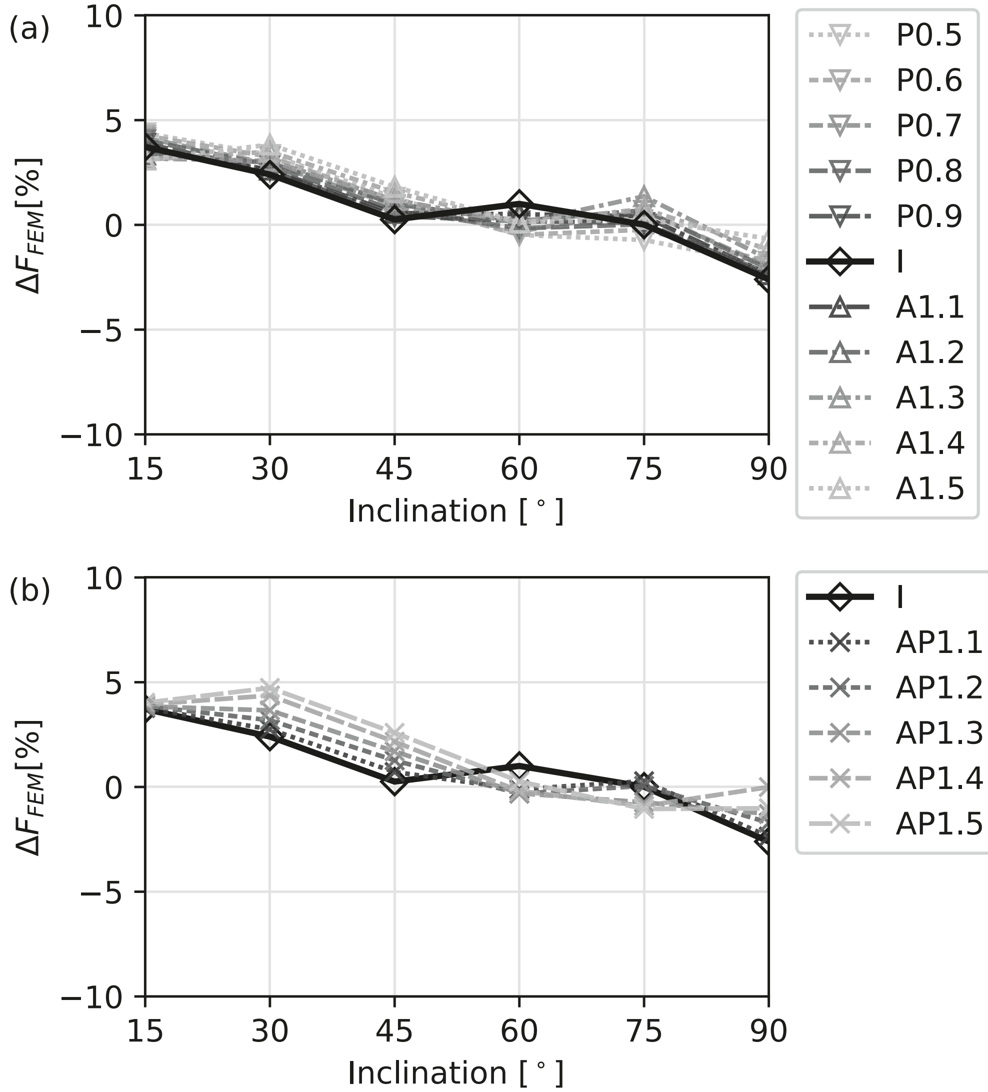

Fig. 12. Failure modes with AP1.5 for homogeneous soil. Solid lines are results from discontinuity layout optimisation and black-white gradients are the normalised incremental deviatoric strain ($\Delta\gamma_s/\Delta\gamma_{s,\,\max}$) from finite element method.

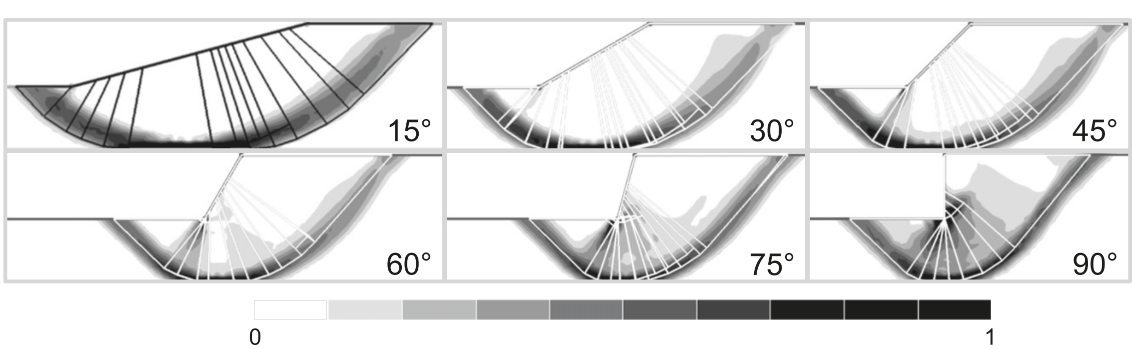

simulations with LimitState:GEO were up to five times faster than the FE analysis in PLAXIS 2D. In comparison with LEM in SLOPE/W, the simulations took three times longer using LimitState:GEO.

5. Conclusion

This study investigates the performance of an anisotropic version of DLO, which is an upper bound approach. The

Fig. 13. Difference in safety factors between discontinuity layout optimisation and finite element method for linearly increasing strength with varying slope inclination for anisotropy applied on (*a*) s_u^A or s_u^P; (*b*) s_u^A and s_u^P.

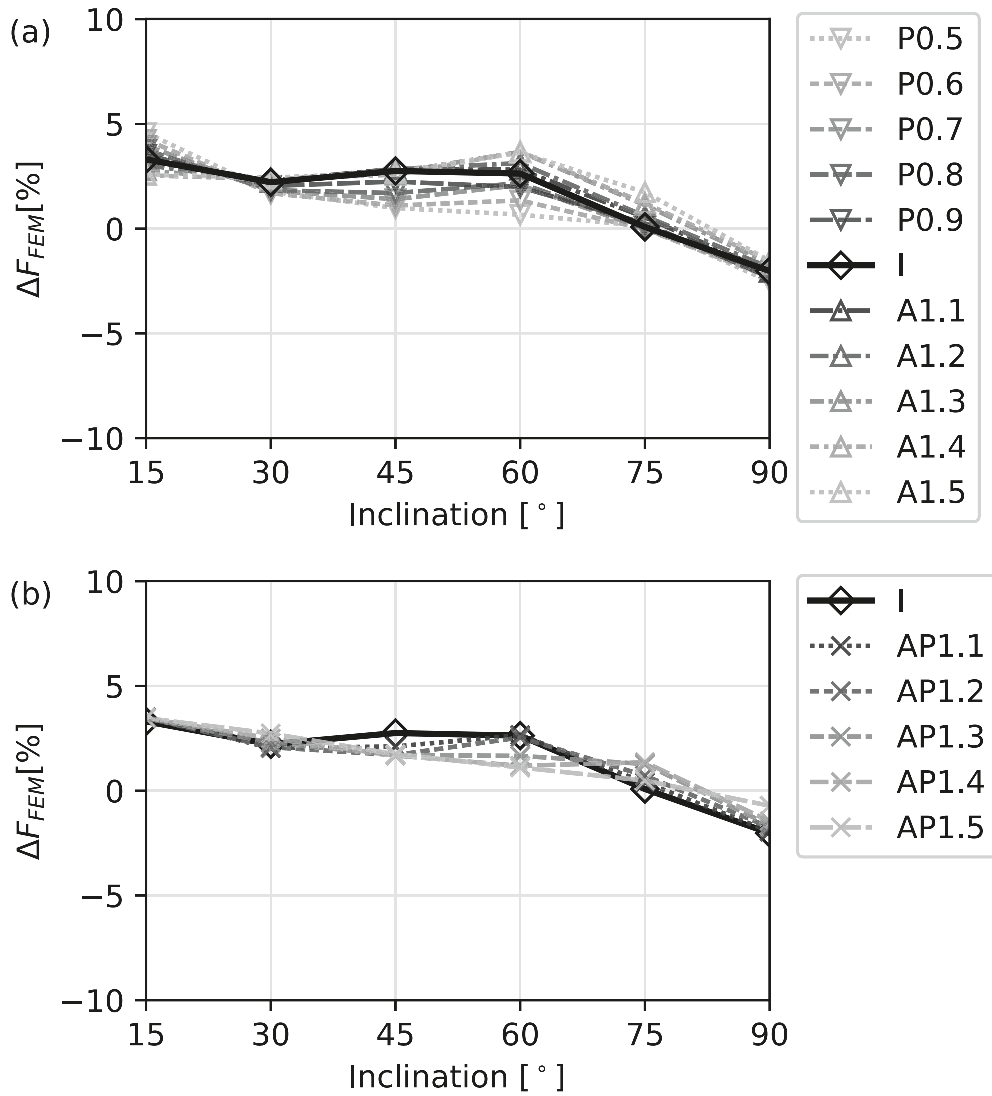

Fig. 14. Example of the element distribution in the finite element models with increased mesh density in weak layer.

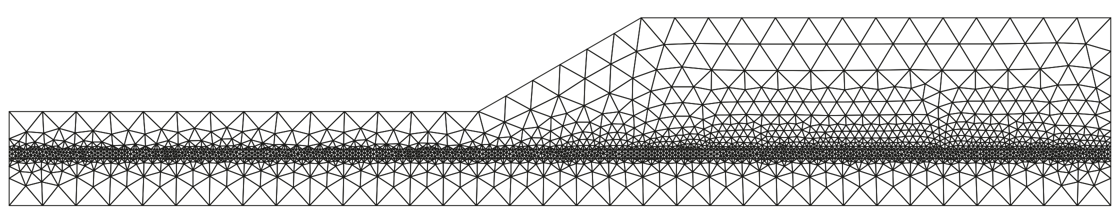

anisotropic failure criterion used is similar to the total-stress based NGI-ADP model implemented in FEM. Subsequently, the anisotropic DLO approach was benchmarked against the NGI-ADP model for slope stability problems. Three idealised cases were used: (1) constant shear strength; (2) linear increase of shear strength with level; and (3) linear increase of shear strength with level with an additional weak layer; all analysed with a reference isotropic shear strength and 15 anisotropic shear strength combinations. The case of constant shear strength was also compared with LEM using Morgenstern–Price method and its user-defined anisotropy.

The results show that the safety factor with anisotropic DLO was predicted to deviate 3%–5% from the numerical implementation in FE, with a general (expected) over-estimation of the safety using DLO. The translational DLO procedure used in this paper did not capture rotational failure modes in the active shear zone, but instead predicted a large wedge that overlapped the rotational mechanism, leading to a

Fig. 15. Difference in safety factors between discontinuity layout optimisation and finite element method for model with weak layer with varying slope inclination for anisotropy applied on (*a*) s_u^A or s_u^P; (*b*) s_u^A and s_u^P.

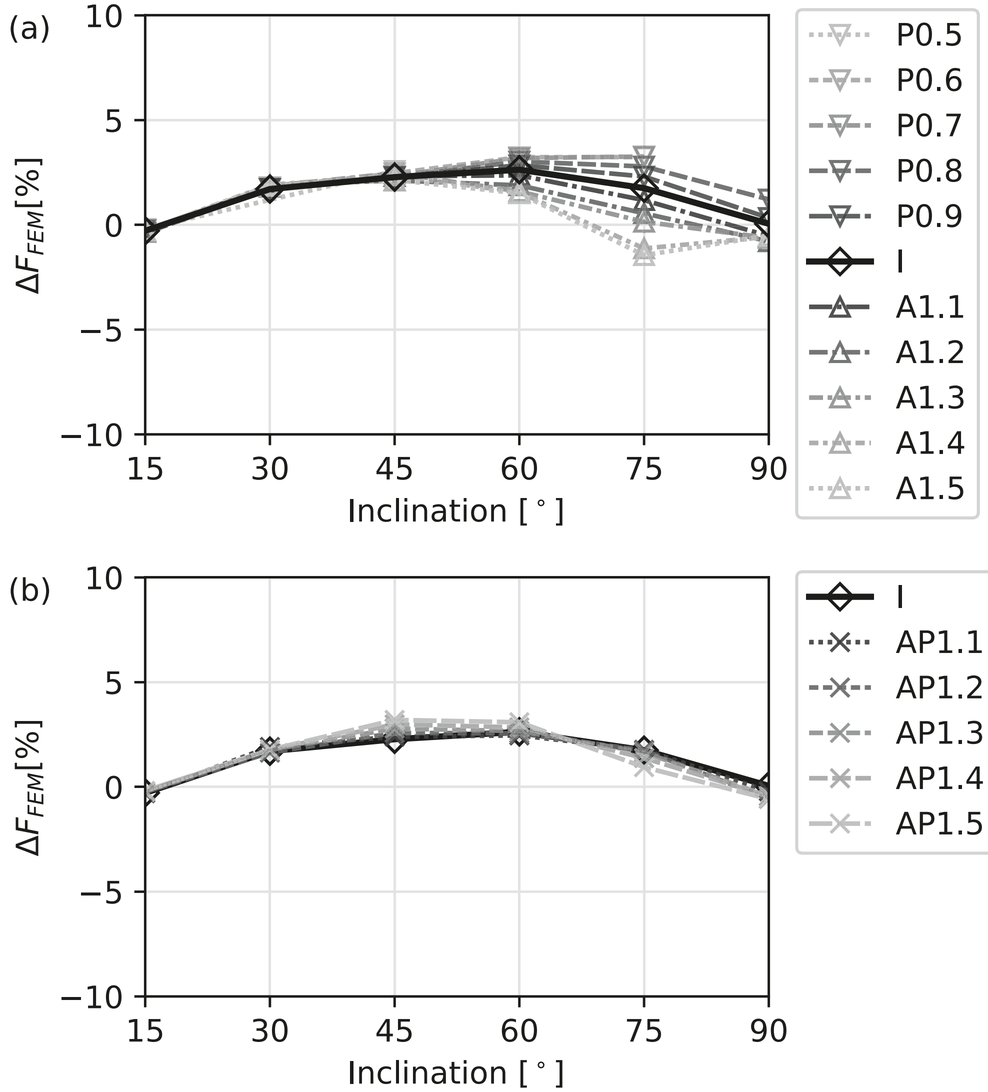

Fig. 16. Failure modes with AP1.5 and a weak layer. Solid lines are results from discontinuity layout optimisation and black–white gradients are the normalised incremental deviatoric strain ($\Delta\gamma_s/\Delta\gamma_{s,\,\max}$) from finite element method.

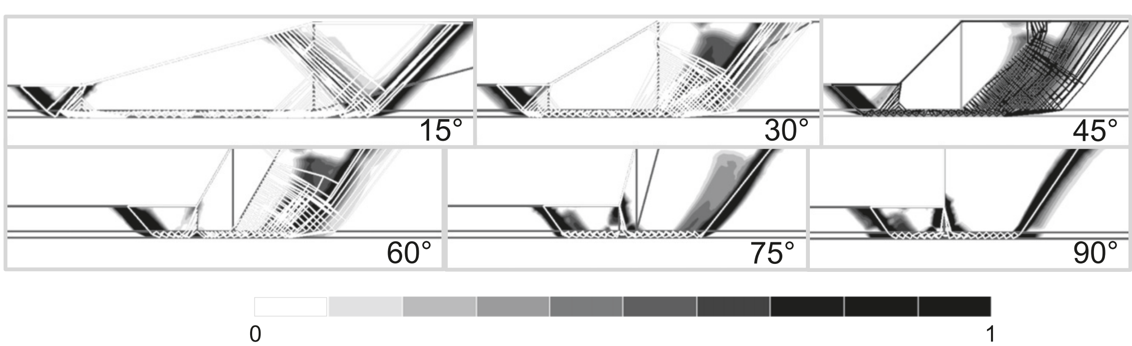

slight overestimation of the safety factor. The inclusion of internal boundaries with rotational failure will likely reduce this overestimation, as shown in the case with a weak layer.

The results highlight the use of DLO as a powerful tool for capturing valid failure modes and safety factors for complex geometries with straight-forward input parameters and low computational time. Furthermore, the method of DLO satisfies the global force equilibrium equations, in contrast to LEM, and is shown to be capable of including total stress anisotropy in a rigorous manner. Additionally, the slip-line-based discretisation efficiently circumvents the problems with numerical convergence that occurs for most FE methods when using plasticity models.

Acknowledgments

The financial support from Trafikverket in the framework of BIG (Branschsamverkan i Grunden), NordForsk (project #98335 NordicLink), and Formas (2021-02400) is greatly acknowledged. The work is done as part of Digital Twin Cities Centre that is supported by Sweden's Innovation Agency VINNOVA. Colin Smith is a director of LimitState Ltd.

Article information

History dates

Received: 13 September 2024
Accepted: 7 May 2025
Accepted manuscript online: 8 May 2025
Version of record online: 13 June 2025

Copyright

Data availability

Data generated or analyzed during this study are available from the first author upon reasonable request.

Author information

Author ORCIDs

Ayman Abed https://orcid.org/0000-0002-5336-3046
Jelke Dijkstra https://orcid.org/0000-0003-3792-0727
Colin Campbell Smith https://orcid.org/0000-0002-0611-9227

Author contributions

Conceptualization: CS, AA, MK, JD, CCS
Formal analysis: CS
Investigation: CS
Methodology: CS, AA, JD
Project administration: AA
Software: CS, CCS
Supervision: AA, MK, JD, CCS
Validation: CS
Visualization: CS
Writing – original draft: CS
Writing – review & editing: AA, MK, JD, CCS

Competing interests

The authors declare there are no competing interests.

References

Billington, E.W. 1988. Generalized isotropic yield criterion for incompressible materials. Acta Mechanica, **72**(1): 1–20. doi:10.1007/BF01176540.

Bishop, A.W. 1955. The use of the slip circle in the stability analysis of slopes. Géotechnique, **5**(1): 7–17. doi:10.1680/geot.1955.5.1.7.

Bjerrum, L. 1973. Problems of soil mechanics and construction on soft clays and structurally unstable soils-collapsible expansive and others. State-of-the-art report to session IV. *In* 8th International Conference on Soil Mechanics and Foundation Engineering. Moscow. pp. 111–159.

Crumpton, M. 2020. Adaptive discontinuity layout optimisation for geotechnical stability analysis. Ph.D. thesis, The University of Newcastle.

Davis, E.H., and Christian, J.T. 1971. Bearing capacity of anisotropic cohesive soil. Journal of the Soil Mechanics and Foundations Division, **97**(5): 753–769. doi:10.1061/JSFEAQ.0001594.

D'Ignazio, M., Länsivaara, T.T., and Jostad, H.P. 2017. Failure in anisotropic sensitive clays: finite element study of Perniö failure test. Canadian Geotechnical Journal, **54**(7): 1013–1033. doi:10.1139/cgj-2015-0313.

Fellenius, W. 1926. Jordstatiska beräkningar med friktion och kohesion (adhesion) och under antagande av cirkulärcylindriska glidytor. Kungl. Väg- och Vattenbyggarkåren 1851-1926, festskrift, Stockholm **22/12**: 79–127.

Georgiadis, K. 2010. Undrained bearing capacity of strip footings on slopes. Journal of Geotechnical and Geoenvironmental Engineering, **136**(5): 677–685. doi:10.1061/(ASCE)GT.1943-5606.0000269.

Gilbert, M., Smith, C.C., Haslam, I.W., and Pritchard, T.J. 2010. Application of discontinuity layout optimization to geotechnical limit analysis problems. In Proceedings of the 7th European Conference on Numerical Methods in Geotechnical Engineering. *Edited by* T. Benz and S. Nordal. CRC Press, Trondheim. pp. 169–174.

Gourvenec, S.M., and Mana, D.S.K. 2011. Undrained vertical bearing capacity factors for shallow foundations. Géotechnique Letters,**1**(4): 101–108. doi:10.1680/geolett.11.00026.

Griffiths, D.V., and Lane, P.A. 1999. Slope stability analysis by finite elements. Géotechnique, **49**(3): 387–403. doi:10.1680/geot.1999.49.3.387.

Grimstad, G., Andresen, L., and Jostad, H.P. 2012. NGI-ADP: anisotropic shear strength model for clay. International Journal for Numerical and Analytical Methods in Geomechanics, **36**(4):483–497. doi:10.1002/nag.1016.

Hird, C.C. 1986. Stability charts for reinforced embankments on soft ground. Geotextiles and Geomembranes, **4**(2): 107–127. doi:10.1016/0266-1144(86)90019-1.

Jewell, R. 1988. The mechanics of reinforcede bankments on soft soils. Geotextiles and Geomembranes, **7**(4): 237–273. doi:10.1016/0266-1144(88)90001-5.

Jostad, H.P., Fornes, P., and Thakur, V. 2014. Effect of strain-softening in design of fills on gently inclined areas with soft sensitive clays. *In* Landslides in sensitive clays: from geosciences to risk management. Edited by J.S. L'Heureux, A. Locat, S. Leroueil, D. Demers and J. Locat, Springer Netherlands, Dordrecht. pp. 305–316. doi:10.1007/978-94-007-7079-9_24.

Karlsrud, K., Lunne, T., Kort, D.A., and Strandvik, S. 2005. CPTU correlations for clays. Proceedings of the 16th International Conference on Soil Mechanics and Geotechnical Engineering, **2**: 693–702. doi:10.3233/978-1-61499-656-9-693.

Krabbenhøft, K. 2023. Finite element limit analysis: fundamentals and extensions. Rev. Fr. Geotech,(175): 5. doi:10.1051/geotech/2023014.

Ladd, C., Foott, R., Ishihara, K., Schlosser, F., and Poulos, H. 1977. Stress-deformation and strength characteristics. *In* Proceedings of the 9th International Conference on Soil Mechanics and Foundation Engineering. Tokyo, Japan. pp. 421–494.

Lee, J.K., Jeong, S., and Ko, J. 2014. Undrained stability of surface strip footings above voids. Computers and Geotechnics, **62**: 128–135. doi:10.1016/j.compgeo.2014.07.009.

Leshchinsky, B. 2013. Comparison of limit equilibrium and limit analysis for complex slopes. *In* Geo-Congress 2013: Stability and Performance of Slopes and Embankments III. pp. 1280–1289. doi:10.1061/9780784412787.129.

Leshchinsky, B. 2015. Bearing capacity of footings placed adjacent to c'-ϕ' slopes. Journal of Geotechnical and Geoenvironmental Engineering, **141**(6). doi:10.1061/(ASCE)GT.1943-5606.0001306.

Leshchinsky, B., and Ambauen, S. 2015. Limit equilibrium and limit analysis: comparison of benchmark slope stability problems. Journal of Geotechnical and Geoenvironmental Engineering, **141**(10): 04015043. doi:10.1061/(ASCE)GT.1943-5606.0001347.

Li, Y., Zhang, W., and Zhang, R. 2022. Numerical investigation on performance of braced excavation considering soil stress-induced anisotropy. Acta Geotechnica, **17**(2): 563–575. doi:10.1007/s11440-021-01171-3.

Liang, T., and Knappett, J.A. 2017. Newmark sliding block model for predicting the seismic performance of vegetated slopes. Soil Dynamics and Earthquake Engineering, **101**(March 2016): 27–40. doi:10.1016/j.soildyn.2017.07.010.

Lo, K. 1965. Stability of slopes in anisotropic soils. Journal of the Soil Mechanics and Foundations Division, **91**(4): 85–106. doi:10.1061/JSFEAQ.0000778.

Loukidis, D., Chakraborty, T., and Salgado, R. 2008. Bearing capacity of strip footings on purely frictional soil under eccentric and inclined loads. Canadian Geotechnical Journal, **45**(6): 768–787. doi:10.1139/T08-015.

Michalowski, R.L. 1989. Three-dimensional analysis of locally loaded slopes. Géotechnique, **39**(1): 27–38. doi:10.1680/geot.1989.39.1.27.

Morgenstern, N.R., and Price, V.E. 1965. The analysis of the stability of general slip surfaces. Géotechnique, **15**(1): 79–93. doi:10.1680/geot.1965.15.1.79.

Mróz, Z., and Drescher, A. 1969. Limit plasticity approach to some cases of flow of bulk solids. Journal of Manufacturing Science and Engineering, **91**(2): 357–364.

Phoon, K.K., and Kulhawy, F.H. 1999. Characterization of geotechnical variability. Canadian Geotechnical Journal, **36**(4): 612–624. doi:10.1139/t99-038.

Rowe, R.K., and Li, A.L. 1999. Reinforced embankments over soft foundations under undrained and partially drained conditions. Geotextiles and Geomembranes, **17**(3): 129–146. doi:10.1016/S0266-1144(98)00035-1.

Rowe, R.K., and Soderman, K.L. 1987. Stabilization of very soft soils using high strength geosynthetics: the role of finite element analyses. Geotextiles and Geomembranes, **6**(1-3): 53–80. doi:10.1016/0266-1144(87)90057-4.

Sambhandharaksa, S. 1977. Stress-strain-strength anisotropy of varved clays. Ph.D. thesis, Massachusetts Institute of Technology.

Skredkommissionen, 1995. Anvisningar för släntstabilitetsutredningar Rapport 3:95. Technical report, Statens Geotekniska Institut, Linköping.

Sloan, S.W. 2013. Geotechnical stability analysis. Géotechnique, **63**(7): 531–572. doi:10.1680/geot.12.RL.001.

Smith, C., and Gilbert, M. 2007. Application of discontinuity layout optimization to plane plasticity problems. Proceedings of the Royal Society A: Mathematical, Physical and Engineering Sciences, **463**(2086): 2461–2484. doi:10.1098/rspa.2006.1788.

Smith, C.C., and Gilbert, M. 2013. Identification of rotational failure mechanisms in cohesive media using discontinuity layout optimisation. Geotechnique, **63**(14): 1194–1208. doi:10.1680/geot.12.P.082.

Smith, C.C., and Gilbert, M. 2022. The stress function basis of the upper bound theorem of plasticity. International Journal of Solids and Structures, **244-245**(July 2021): 111565. doi:10.1016/j.ijsolstr.2022.111565.

Smith, C.C., and Tatari, A. 2016. Limit analysis of reinforced embankments on soft soil. Geotextiles and Geomembranes, **44**(4): 504–514. doi:10.1016/j.geotexmem.2016.01.008.

Spencer, E. 1967. A method of analysis of the stability of embankments assuming parallel inter-slice forces. Géotechnique, **17**(1): 11–26. doi:10.1680/geot.1967.17.1.11.

Ukritchon, B., and Boonyatee, T. 2015. Soil parameter optimization of the NGI-ADP constitutive model for Bangkok soft clay. Geotechnical Engineering of the SEAGS & AGSSEA, **46**(1): 28–36.

Vahedifard, F., Shahrokhabadi, S., and Leshchinsky, D. 2016. Optimal profile for concave slopes under static and seismic conditions. Canadian Geotechnical Journal, **53**(9): 1522–1532. doi:10.1139/cgj-2016-0057.

Yang, S., Leshchinsky, B., Cui, K., Zhang, F., and Gao, Y. 2019. Unified approach toward evaluating bearing capacity of shallow foundations near slopes. Journal of Geotechnical and Geoenvironmental Engineering, **145**(12): 1–16. doi:10.1061/(ASCE)GT.1943-5606.0002178.

Yu, H.S., Salgado, R., Sloan, S.W., and Kim, J.M. 1998. Limit analysis versus limit equilibrium for slope stability. Journal of Geotechnical and Geoenvironmental Engineering, **124**(1): 1–11. doi:10.1061/(ASCE)1090-0241(1998)124:1(1).

Zheng, G., Zhao, J., Zhou, H., and Zhang, T. 2019. Ultimate bearing capacity of strip footings on sand overlying clay under inclined loading. Computers and Geotechnics, **106**: 266–273. doi:10.1016/j.compgeo.2018.11.003.

Zheng, G., Yu, X., Zhou, H., Wang, S., Zhao, J., He, X., and Yang, X. 2020. Stability analysis of stone column-supported and geosynthetic-reinforced embankments on soft ground. Geotextiles and Geomembranes, **48**(3): 349–356. doi:10.1016/j.geotexmem.2019.12.006.

Zhou, H., Zheng, G., He, X., Xu, X., Zhang, T., and Yang, X. 2018a. Bearing capacity of strip footings on c–ϕ soils with square voids. Acta Geotechnica, **13**(3): 747–755. doi:10.1007/s11440-018-0630-0.

Zhou, H., Zheng, G., Yin, X., Jia, R., and Yang, X. 2018b. The bearing capacity and failure mechanism of a vertically loaded strip footing placed on the top of slopes. Computers and Geotechnics, **94**: 12–21. doi:10.1016/j.compgeo.2017.08.009.

Zhu, H.H., Wang, Z.Y., Shi, B., and Wong, J.K.W. 2016. Feasibility study of strain based stability evaluation of locally loaded slopes: Insights from physical and numerical modeling. Engineering Geology, **208**: 39–50. doi:10.1016/j.enggeo.2016.04.019.

Zienkiewicz, O.C., Humpheson, C., and Lewis, R.W. 1975. Associated and non-associated visco-plasticity and plasticity in soil mechanics. Géotechnique, **25**(4): 671–689. doi:10.1680/geot.1975.25.4.671.

Appendix A. Derivation of $\widehat{J_2}$ and $\widehat{J_3}$

Modified Cartesian stress component:

$$\text{(A1)} \quad \widehat{\sigma}'_{ii} = \sigma'_{ii} - \sigma'_{ii0}\,(1-\kappa)$$

where $i = [x, y, z]$ and 0 indicate initial stress.

Modified mean stress:

$$\text{(A2)} \quad \widehat{p} = \frac{\widehat{\sigma}'_{xx} + \widehat{\sigma}'_{yy} + \widehat{\sigma}'_{zz}}{3} = p' - (1-\kappa)\,p'_0$$

Modified deviatoric stress vector (Grimstad et al. 2012):

$$\text{(A3)} \quad \begin{bmatrix} \widehat{s}_{xx} \\ \widehat{s}_{yy} \\ \widehat{s}_{zz} \\ \widehat{s}_{xy} \\ \widehat{s}_{xz} \\ \widehat{s}_{yz} \end{bmatrix} = \begin{bmatrix} \widehat{\sigma}'_{xx} + \kappa\dfrac{1}{3}\left(s_u^A - s_u^P\right) - \widehat{p} \\ \widehat{\sigma}'_{yy} - \kappa\dfrac{2}{3}\left(s_u^A - s_u^P\right) - \widehat{p} \\ \widehat{\sigma}'_{zz} + \kappa\dfrac{1}{3}\left(s_u^A - s_u^P\right) - \widehat{p} \\ \tau_{xy}\cdot\dfrac{s_u^A + s_u^P}{2s_u^{DSS}} \\ \tau_{xz} \\ \tau_{yz}\cdot\dfrac{s_u^A + s_u^P}{2s_u^{DSS}} \end{bmatrix}$$

Modified second and third deviatoric invariants:

$$\text{(A4)} \quad \widehat{J_2} = -\widehat{s}_{xx}\widehat{s}_{yy} - \widehat{s}_{xx}\widehat{s}_{zz} - \widehat{s}_{yy}\widehat{s}_{zz} + \widehat{s}^2_{xy} + \widehat{s}^2_{xz} + \widehat{s}^2_{yz}$$

$$\text{(A5)} \quad \widehat{J_3} = -\widehat{s}_{xx}\widehat{s}_{yy}\widehat{s}_{zz} + 2\widehat{s}_{xy}\widehat{s}_{yz}\widehat{s}_{zx} - \widehat{s}_{xx}\widehat{s}^2_{yz} - \widehat{s}_{yy}\widehat{s}^2_{xz} - \widehat{s}_{zz}\widehat{s}^2_{xy}$$

Appendix B. Safety factors

Figures B1, B2, B3 and B4 present the calculated safety factors from each method (i.e., LEM, DLO, and FEM) with back-

Fig. B1. F_{DLO} (numerator) and F_{LEM} (denominator) for homogeneous soil.

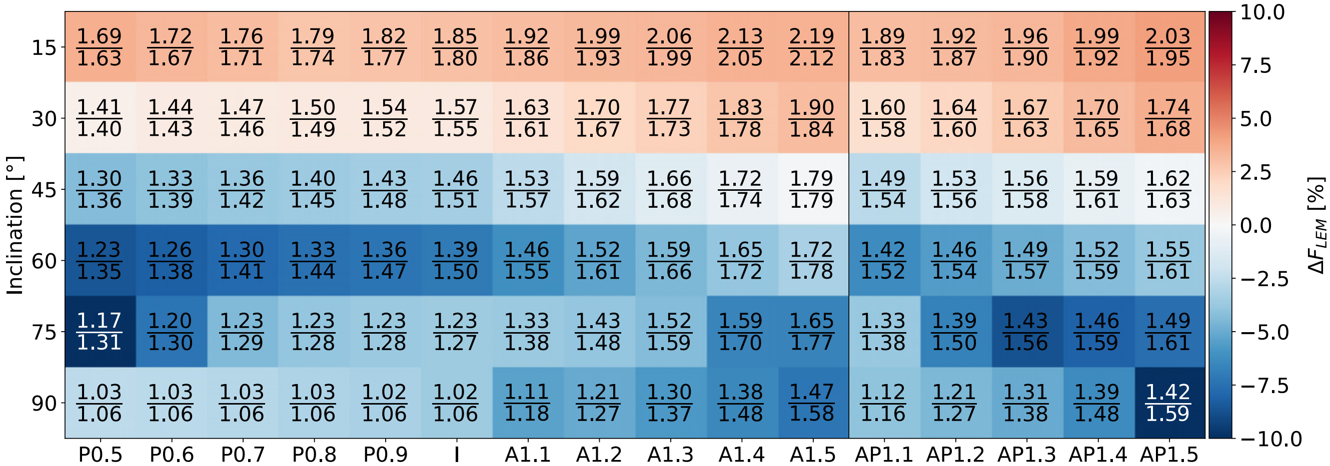

Fig. B2. F_{DLO} (numerator) and F_{FEM} (denominator) for homogeneous soil.

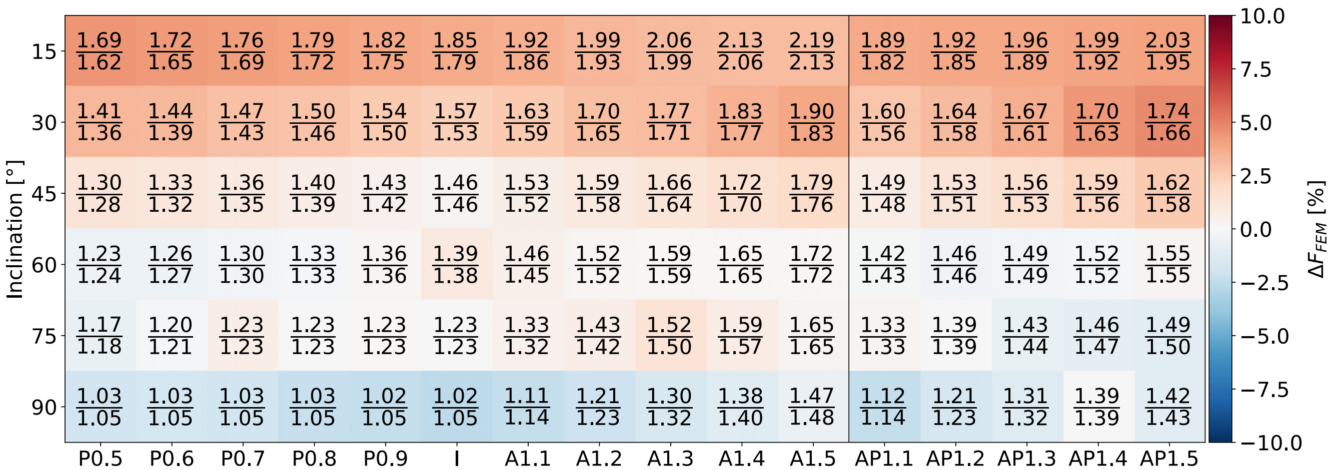

Fig. B3. F_{DLO} (numerator) and F_{FEM} (denominator) for homogeneous soil with linearly increasing strength.

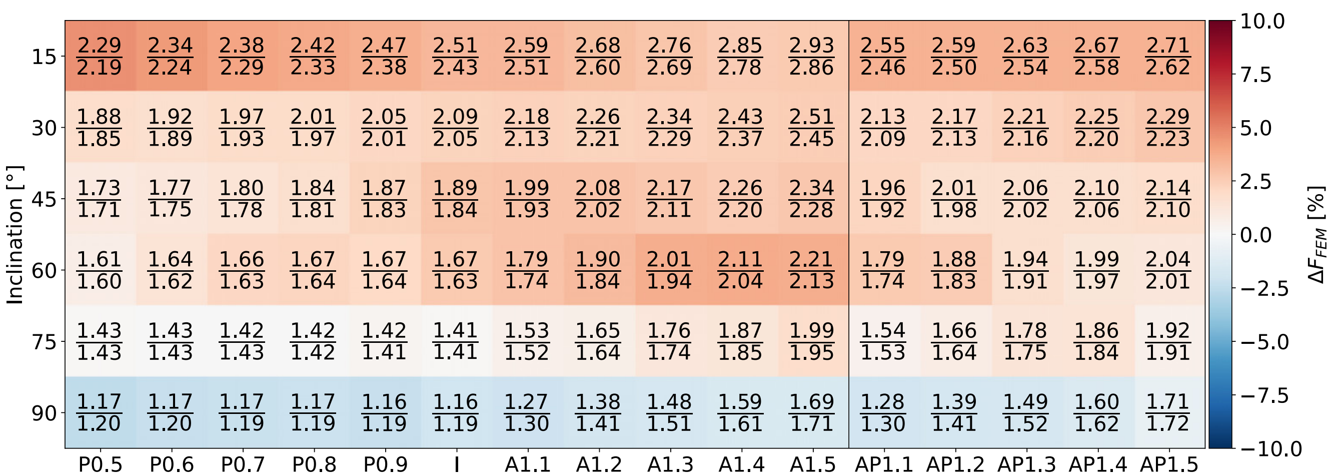

ground colour visualising the relative difference between them, see eq. 11. In Fig. B4, the white boxes mean that no F_{FEM} was obtained, since $F_{\mathrm{FEM}} < 1.0$ and the highlighted black solid frames mark the calculations in LimitState:GEO where a safety factor could only be obtained by an increase of gravity, and not from strength reduction. In theory, the two different methods should result in the same safety factor for undrained conditions.

 Can. Geotech. J. 62: 1–16 (2025) | dx.doi.org/10.1139/cgj-2024-0541

Fig. B4. F_{DLO} (numerator) and F_{FEM} (denominator) for model with weak layer.

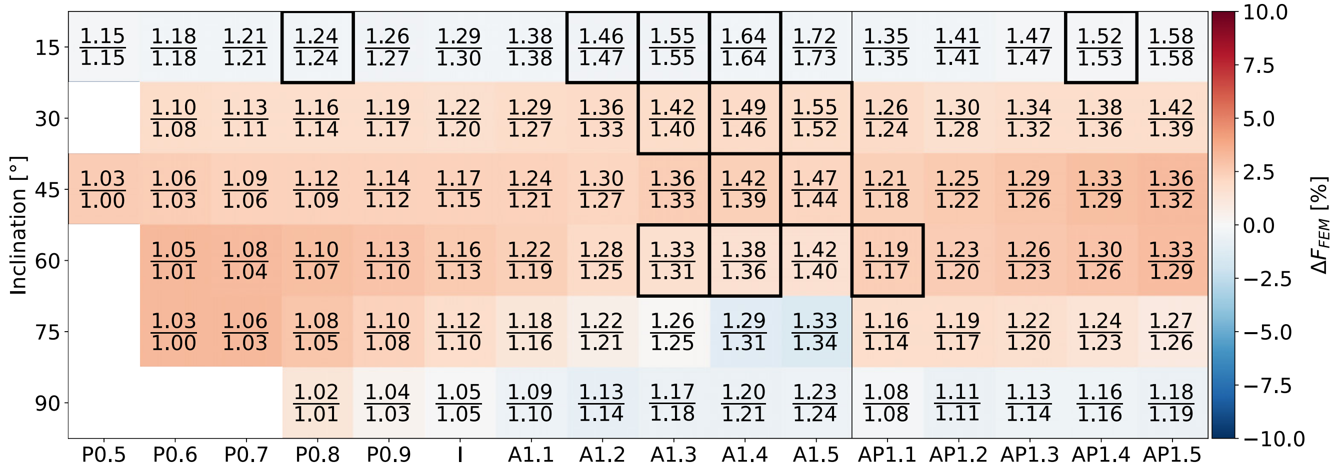

Appendix C. Rotational failure along boundaries

LimitState:GEO allows for modelling rotational failure along boundaries, to account for rotating structural elements or anticipated local soil rotations. The boundaries allow the adjacent (rigid) blocks to rotate along the boundary, generally with a log-spiral failure mechanism, and convert it to approximate translational deformations acting on adjacent, nonboundary, blocks. This principal is based on the assumption that the rotating blocks are small, and any application thereby requires a high nodal density along the boundary. Figure C1 shows the internal boundaries used for the scenario with a weak layer.

Fig. C1. Illustration of the internal boundaries. Inclined internal boundary is set to be parallel to slope inclination.

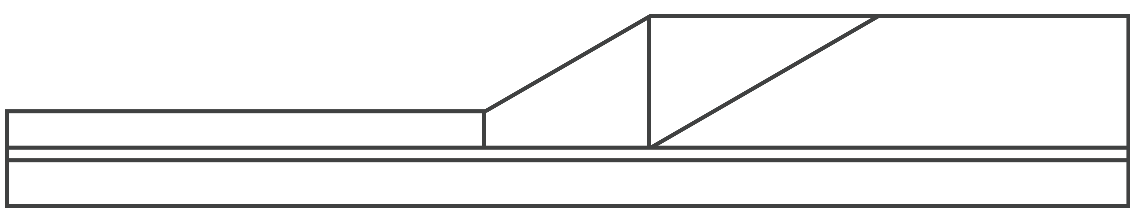

Appendix D. Effect of level-dependent shear strength

Fig. D1. Illustration of how the anisotropic ratio varies with failure level and failure mode, with the consistent relation $s_u^P/s_u^A < s_{uL}^P/s_{uL}^A < 1$.